SCIENTIFIC REPORTS
nature research

Check for updates

OPEN

Computational studies on the gas phase reaction of methylenimine (CH_2NH) with water molecules

Mohamad Akbar Ali

In this work, we used quantum chemical methods and chemical kinetic models to answer the question of whether or not formaldehyde (CH_2O) and ammonia (NH_3) can be produced from gas phase hydration of methylenimine (CH_2NH). The potential energy surfaces (PESs) of $CH_2NH + H_2O \rightarrow CH_2O + NH_3$ and $CH_2NH + 2H_2O \rightarrow CH_2O + NH_3 + H_2O$ reactions were computed using CCSD(T)/6–311++G(3d,3pd)// M06-2X/6–311++G(3d,3pd) level. The temperature-and pressure-dependent rate constants were calculated using variational transition state theory (VTST), microcanonical variational transition state theory ($\mu VTST$) and Rice–Ramsperger–Kassel–Marcus/master equation (RRKM/ME) simulations. The PES along the reaction path forming a weakly bound complex ($CH_2NH\cdots H_2O$) was located using VTST and μVTST, however, the PES along the tight transition state was characterized by VTST with small curvature tunneling (SCT) approach. The results show that the formation of $CH_2NH + H_2O \rightarrow CH_2NH\cdots H_2O$ is pressure -and temperature-dependent. The calculated atmospheric lifetimes of $CH_2NH\cdots H_2O$ (~ 8 min) are too short to undergo secondary bimolecular reactions with other atmospheric species. Our results suggest that the formation of CH_2O and NH_3 likely to occur in the combustion of biomass burning but the rate of formation CH_2O and NH_3 is predicted to be negligible under atmospheric conditions. When a second water molecule is added to the reaction, the results suggest that the rates of formation of CH_2O and NH_3 remain negligible.

The alkylamines especially methylamine is emitted to the atmosphere from various sources such as biogenic, oceanic, anthropogenic, animal husbandry, marine emissions, biomass burning (forest vegetation, savannah grass, firewood and agricultural wastes), chemical manufacturing and carbon capture storage (CCS) technologies[1].

Methylamine (CH_3NH_2) is one of the atmospheric precursors of the greenhouse nitrous oxide (N_2O) gas and HCN and is one of the sources of the formation of NO_x[2–4]. For example: the synthetic nitrogen-based fuel is one the source of NO_x emission[5,6]. Methylamine has also received numerous attention due to its potential role in enhancing particle nucleation and growth and affecting secondary organic aerosol (SOA) formation[7,8]. After emission into the atmosphere, methylamine undergoes conversion reactions in both the gas and aqueous phases. The gas phase reaction of methylamine with hydroxyl radical ($CH_3NH_2 + OH$) is the most important pathway of degradation of methylamine[9,10]. The OH radical initially abstracts the hydrogen from the C–H and N–H groups of the methylamine to generate carbon-centered aminomethyl radical ($\cdot CH_2NH_2$) as a major product and nitrogen-centered methylamine radical ($CH_2N\cdot H$) as a minor product[10]. The major detected products from the photooxidation of methylamine are 90% methylenimine (CH_2NH) and ~ 10% nitrosamine, a carcinogen. The photooxidation reaction of methylamine is given below[1,9,10]

$$CH_3NH_2 + \cdot OH \rightarrow \cdot CH_2NH_2 + H_2O \quad (1)$$

$$\cdot CH_2NH_2 + O_2 \rightarrow \cdot OOCH_2NH_2 \quad (2)$$

$$\cdot OOCH_2NH_2 \rightarrow HOOCH_2NH\cdot \quad (3)$$

$$HOOCH_2NH\cdot \rightarrow CH_2NH + HO_2\cdot \quad (4)$$

Department of Chemistry, College of Science, King Faisal University, 31982, Al-Ahsa, Saudi Arabia. email: aamohamad@kfu.edu.sa

Methylenimine has been identified as a potential prebiotic precursor of glycine, and it has been detected spectroscopically in interstellar clouds[11,12]. Methylenimine can also be produced from the decomposition of methyl azides[4] and 2-azidoacetic acid[13]. Experimental study on the electronic spectrum of CH_2NH shows the broad absorption of the spectrum of $n \rightarrow \pi^*$ transition in the region 235–260 nm with the maximum absorption cross-section of $\sim 4 \times 10^{-19}$ cm^2 $molecule^{-1}$ near 250 nm[14]. In another experimental study, Rissanen et al.[10] used photoionization mass spectrometry to detect the formation of CH_2NH from $CH_2NH_2 + O_2$ reaction[10]. Methylenimine is isoelectronic with both formaldehyde and ethylene, therefore it can react in several ways. Various research groups have been predicted the structural and thermochemical properties of reverse reaction i.e., $CH_2O + NH_3 \rightarrow CH_2NH + H_2O$[15–20]. But the atmospheric fate of CH_2NH with H_2O is not known with certainty because no direct measurements of its reaction kinetics have been carried out. Recently, we have computed the rate constants for $CH_2O + NH_3$ reaction using ab initio/DFT methods coupled with statistical rate theory[20]. We have proposed the formation of $CH_2O\cdots NH_3$, NH_2CH_2OH and CH_2NH from $CH_2O + NH_3$ reaction.

There has been considerable speculation about the atmospheric reaction of methylenimine because this compound is highly reactive, soluble in water, and sticky, thus posing severe experimental challenge[1,21–25]. Some researchers suggested that methylenimine can be either photo-oxidized or can react with water vapor[1,21–25]. Gas-phase theoretical models of the methylenimine chemistry in hot protostellar cores are required to explain the formation of substantially larger organics under interstellar conditions[26]. These molecules can then undergo gas-phase reactions to form more complex species such as amino acids, sugars, and other biologically important molecules surface. For example, the formation of aminomethanol (NH_2CH_2OH) from $CH_2NH + H_2O$ reaction, which can further react with formic acid (HCOOH) to produce glycine and alanine.

Theoretical studies on the atmospheric degradation of methylenimine initiated by HO and HO_2 radicals have been performed by various research groups[21–25]. In 2015, Ali and Barker predicted the rate constants for the $OH + CH_2NH$ reaction using ab initio//DFT methods coupled with variational transition state theory[21]. We suggested that $OH + CH_2NH$ has similarities with its isoelectronic analogous $OH + CH_2O$ and $OH + CH_2CH_2$ reactions. The reaction rate constants were predicted in the range of 10^{-11} to 10^{-12} cm^3 $molecule^{-1}$ s^{-1} under atmospheric condition. In 2016, Vazart et al.[26] calculated the rate constants for $OH + CH_2NH$ reaction using DFT and CCSD(T) level. Our group has also predicted the rate constants for $HO_2 + CH_2NH$ reaction using ab initio//DFT methods coupled with microcanonical variational transition state theory[22]. Recently, Ali et al.[23,24] proposed the reaction mechanism of the catalytic effect of a single water molecule on the $OH + CH_2NH$, $OH + CH_2O$ and $OH + CH_2CH_2$ reactions. Ali et al.[23,24] concluded that a single water molecule has a negative effect on $OH + CH_2NH$, $OH + CH_2O$ and $OH + CH_2CH_2$ reactions. Ali et al. suggested that water-assisted $OH + CH_2NH$, $OH + CH_2O$ and $OH + CH_2CH_2$ reactions cannot accelerate the reaction because the dominated water-assisted process depends parametrically on water concentration. As a result, the overall reaction rate constants are smaller[23,24].

In earlier studies[1,10,27], various research groups have been proposed that the hydrolysis of methylenimine will produce $CH_2O + NH_3$, but no clear justification has been made so far. They suggested that, CH_2NH are water-soluble and will be absorbed by aqueous aerosols in the troposphere. In aqueous solution, it is well known that CH_2NH undergoes hydrolysis to yield ammonia and formaldehyde. The process of formation of ammonia and formaldehyde is acid-catalyzed and should be relatively rapid in aerosol droplets[1,10,27]. The interest of present work is to address the question of whether the gas phase reaction of CH_2NH with H_2O will leads to the formation of formaldehyde and ammonia.

The role of the water molecule as a catalyst in the hydrogen transfer reaction of simple atmospheric and combustion product i.e., ketene ($H_2C{=}C{=}O$) has been studied by various research groups[28–30]. Nguyen et al.[28] calculated gas phase pseudo-first-order reaction rate constants for ketene with water molecules at room temperature. The calculated decay rate of ketene was obtained for both the pathways 1.5×10^{-19} (pathway A) and 1.5×10^{-16} s^{-1} (pathway B). They suggested that the gas phase reaction with ketene and water molecules to form acetic acid is many orders of magnitude slower. They also purposed that room-temperature formation of acetic acid from $CH_2CO + 2H_2O \rightarrow NH_3 + CH_2O$ is almost negligible and maybe provide better understanding in the aqueous phase chemistry[28]. The role of two-water reaction with CH_2NH is also of great interest from the viewpoint of atmospheric and combustion chemistry research. Because CH_2NH is also isoelectronic analogous to important atmospheric and combustion species *i.e.,* CH_2O and CH_2CH_2.

To the best of our knowledge, there have been no theoretical chemical kinetics investigations on the hydrolysis of CH_2NH in the gas phase. To investigate the various possibilities of $CH_2NH + H_2O$ and $CH_2NH + 2H_2O$ reactions, we used ab initio/DFT method for the potential energy surface and advanced kinetic models to predict the temperature- and pressure-dependent rate constants. Finally, concluding remark whether the formation of CH_2O and NH_3 is a possible pathway under both atmospheric and combustion conditions are drawn.

Theoretical methods

Electronic structure calculations. Geometries of all stationary points were optimized using M06-2X method[31] in conjunction with Pople 6–311++G(3df,3pd) basis set[32]. The M06-2X has been shown to be reliable for handling noncovalent interactions between molecules and widely used to locate the transition states of atmospheric and combustion reaction systems[20,33–35]. The optimized structure of reactants, complexes, intermediates, and transition states (TSs) are shown in Supporting Information Figure S1 and the cartesian coordinates are given in Supporting Information Table S1. Vibrational frequencies were calculated at M06-2X/6–311++G(3df,3pd) to estimate the zero-point corrections (ZPE) for the reactants, complexes, TSs and products. The frequency calculation also shows that the optimized transition states have single imaginary frequency and reactants, complexes, intermediates and products have all positive vibrational frequencies (see Supporting Information, Table S2). Rotational constants were calculated at the same level to calculate rotational partition

functions (see Supporting Information, Table S3). Intrinsic reaction coordinate (IRC) calculations were carried out at M06-2X/6–311++G(3df,3pd) level to confirm the identities of the reactants and products for every transition state. Single point energy calculations were calculated using CCSD(T)/6–311++G(3df,3pd) level of theory[36–39] (see Supporting Information, Table S4) on M06-2X/6–311++G(3df,3pd) optimized geometries. The combination of CCSD(T)/6–311++G(3df,3pd)//M06-2X/6–311++G(3df,3pd) (designated CC//M06) has been tested by many research groups[20,33–35] and shown to be reasonably accurate. T1 diagnostic was computed using CCSD(T)/6–311++G(3df,3pd) for all important species was < 0.017, which is acceptable for a single reference wave function[40]. The T1 diagnostic for all the species involved in the reaction are given in Supporting Information Table S5. Gaussian 09 suite of programs was used for all ab initio/density functional theory (DFT) calculations[41].

Kinetics. *High-pressure limit rate constants.* The high-pressure limit rate constants for title reaction were calculated using canonical variational transition state theory with small curvature tunneling correction (SCT). The generalized rate constants were calculated by minimizing the transition state dividing surface along the reaction coordinate to get the canonical variational transition state theory (CVT) rate constants, which is given by Eqs. (5) and (6):

$$k^{GT}(T,\ s) = \Gamma L^{\neq} \times \frac{k_B T}{h} \frac{Q^{\neq}_{TS}(T,\ s)(T,\ s)}{Q_R(T)} exp\left(-\frac{V_{MEP}(s)}{k_B T}\right) \tag{5}$$

$$k^{CVT}(T) = \min_{s} k^{GT}(T,\ s) = k^{GT}(T,\ s^{CVT}(T)) \tag{6}$$

where $k^{GT}(T,\ s)$ and $k^{CVT}(T)$ are the rate constants of generalized and canonical variational, transition state theory, respectively, V_{MEP} is the classical barrier height, Γ is the small curvature tunneling (SCT) correction as implemented in Polyrate[42], h is Planck's constant, k_B is the Boltzmann constant, and $Q^{\neq}_{TS}$ and Q_R are the total partition functions for the transition state and the reactants, respectively. The rate constants were calculated using dual level direct dynamic approach CVT/SCT with interpolated single point energies (ISPE)[43]. The minimum energy pathway is obtained using direct dynamics for a small range of the reaction path with the mass scaled reaction coordinate 's' from − 1.0 to 1.0 bohr by using the Page–McIver integrator with a step size of 0.005 bohr. The SCT transmission coefficients[44], that include the reaction-path curvature effect on the transmission probability, are based on the centrifugal-dominant small-curvature semiclassical adiabatic ground-state (CD-SCSAG) approximation were computed as discussed in Ref.[44]. The SCT method[44] was widely used for many atmospheric and combustion reaction systems and provide reasonably accurate value[23,24,33]. All the unimolecular reaction rate constants for non-barrierless reaction were calculated using Polyrate and Gaussrate suites of program[42,45]. The $K_{eq}(T)$ for all the reactants → complexes and complexes → pre-reactive complex were calculated (see Supporting Information Table S6) using THERMO code as implemented in MultiWell Program suite[46–48]. The details procedure of $K_{eq}(T)$ calculations are given in the Supporting Information.

For barrierless reaction, *ktools* program was used to compute rate constants based on variational transition states theory (VTST) and microcanonical variational transition states theory (μVTST)[46–48]. In the *ktools* program, we supply reactants and the collection of the loose transition states along the reaction coordinate. This can be further achieved by performing a series of constrained optimizations at fixed distances along the reaction path (RP). At each fixed distance, the potential energy was calculated, and optimized geometry was used to obtain the rotational constants and a vibrational analysis was used to obtain the vibrational frequencies of the orthogonal degrees of freedom, after projecting out the reaction coordinate. The zero-point energy from the orthogonal modes, $\Delta E_z(s)$, and the electronic energy $\Delta E_e(s)$ at each fixed bond distance s were used to compute the potential energy with ZPE corrections: $V(s) = \Delta E_e(s) + \Delta E_z(s)$, where $\Delta E_e(s) = E_e(s) - E_e(s=0)$ and $\Delta E_z(s) = E_z(s) - E_z(s=0)$. The rotational partition functions and vibrational partition functions were computed from rotational constants and the vibrational frequencies, respectively for the orthogonal normal modes evaluated at the fixed distance s. Utilizing these parameters, "trial" rate constants or reaction fluxes were computed at each point along the reaction path[20–22]. The point at which the minimum trial rate constant or reaction flux occurs was identified as a variational transition state (VTS). The obtained minimum TS is also compatible to run the master equation (ME) code for pressure- and temperature-dependent rate constants.

Pressure-dependent rate constants. The 2-D microcanonical rate constants, $k_i(E')$ for a specific J' were calculated according to Eq. 7:

$$k(E',\ J') = \frac{L^{\neq}}{h} \times \frac{G^{\neq}(E' - E_0^T,\ J')}{\rho(E',\ J')} \tag{7}$$

where $L^{\neq}$ is the reaction path degeneracy can be written as the product of a ratio of symmetry factors and a ratio of optical isomers; h is Planck's constant; $G^{\neq}(E' - E_0,\ J')$ is the sum of states of the transition state as a function of the active energy $E' - E_0^T$; and E_0^T is the reaction critical energy, which includes zero-point-energy and centrifugal corrections at temperature T; $\rho(E',\ J')$ is the 2-D density of states of the reactant molecule. The microcanonical thermally averaged high-pressure limit rate constants were obtained as discussed in Ali et al. work[22].

For pressure-dependent rate constants, RRKM/ME simulation was used to calculate the rate constants as a function of pressure. The calculated sum of states and density of state from the microcanonical process were used to run master equation (ME) code for pressure-dependent (i.e. falloff curve) rate constants. The vibrational frequencies and the moments of inertia were used to calculate the density of states and the sum of states were based

Reaction species	This work[a]	This work[b]	Riffet et al.[c]	Exp.[d]
$CH_2NH + H_2O$	0.0	0.0	0.0	0.0
$CH_2O + NH_3$	−0.2	−0.4	−0.4	−0.3
$CH_2NH\cdots H_2O$	−6.7	−4.4	−3.8	
$OH\text{-}CH_2\text{-}NH_2$	−14.9, −14.2	−9.6, −8.9	−9.6, −8.8	
$CH_2O\cdots NH_3$	−3.5	−2.1	−2.4	
TS1	45.7	46.4	46.8	
TS2	−10.2	−5.2	−5.0	
TS3	28.8	30.8	31.1	
$CH_2NH + 2H_2O$	0.0	0.0	0.0	0.0
$H_2O\cdots CH_2NH\cdots H_2O$	−16.3	−11.6	−10.3	
$OH\text{-}CH_2\text{-}NH_2\cdots H_2O\text{-}1$	−22.6	−14.9	−14.8	
$OH\text{-}CH_2\text{-}NH_2\cdots H_2O\text{-}2$	−23.9	−15.7	−14.1	
$CH_2O\cdots NH_3\cdots H_2O$	−11.7	−7.6	−6.2	
$TS1\cdots H_2O$	17.7	20.7	21.3	
$TS2\cdots H_2O$	−15.5	−8.5	−8.8	
$TS3\cdots H_2O$	2.9	7.6	7.6	

Table 1. Calculated energies (in kcal/mol) for species associated with the reaction of methylenimine with one-water and two-water molecules. [a]Calculated at CCSD(T)/6–311++G(3df,3pd)//M06-2X/6–311++G(3df,3pd), [b]Calculated at CCSD(T)/6–311++G(3df,3pd)//M06-2X/6–311++G(3df,3pd) + ZPE. [c]Calculated by Riffet et al. work[15]. [d]From ATcT data[52–54].

on the Stein–Rabinovitch version of the Beyer–Swineheart algorithm[49,50]. N_2 gas was used as the bath gas, and the energy transfer model with $\langle \Delta E \rangle_{down} = 200 \times (T/300)^{0.85}$ cm^{-1}[51]. The Lennard–Jones parameters for a N_2 gas ($\sigma = 4.74$ Å and $\varepsilon/k_B = 82$ K) were taken from literature[21] and the Lennard–Jones parameters for all intermediate species ("Well") ($\sigma = 4.94$ Å and $\varepsilon/k_B = 275$ K) were based on the previous study[10]. The initial energy distribution for the simulations was the chemical activation distribution for the combination reaction producing the $CH_2NH\cdots H_2O$. The temperature and pressure-dependent rate constants were obtained using MultiWell code. The rate constants were calculated over the temperature range of 200–350 K at N_2 pressures from 0.01 to 1,000 atm.

Results and discussion

All the stationary points on the PESs for $CH_2NH + H_2O$ reaction were obtained using CC/M06 level. To examine the possible catalytic effect of water molecule on the $CH_2NH + H_2O$ reaction, we explored the PES of the addition of one water molecule. After the depiction of reaction pathways are considered ("Reaction pathways and thermodynamics analysis"), for which temperature and pressure-dependent rate constants predicted, the ensuing "Rate constants" details chemical kinetic results of $CH_2NH + H_2O$ and $CH_2NH + 2H_2O$ reactions and "Atmospheric and combustion implications" describes the atmospheric and combustion implications of $CH_2NH + H_2O$ reaction system.

Reaction pathways and thermodynamics analysis. The hydrolysis of methylenimine forming formaldehyde and ammonia is shown below:

$$H_2C=N-H\,(\text{Methylenimine}) + H_2O \rightarrow OH-H_2C-NH_2\,(\text{Aminomethanol}) \rightarrow CH_2O + NH_3.$$

In the first step, hydrogen transfer from water molecule to methylenimine producing aminomethanol. In the second step, hydrogen transfer from aminomethanol followed by removal of ammonia produces formaldehyde (see the scheme in SI).

The zero-point corrected energies of each stationary point on the PES for the $CH_2NH + H_2O$ reaction are tabulated in Table 1 and shown in Fig. 1. Our calculated reaction enthalpy for $CH_2NH + H_2O \rightarrow CH_2O + NH_3$ (−0.4 kcal/mol) at CC//M06 is in excellent agreement with the experimentally measured value (−0.3 kcal/mol)[52–54]. Our calculated value is also in excellent agreement with the value obtained by Riffet et al.[15]. Both water ($\mu_D = 1.91$D) and methylenimine ($\mu_D = 2.045$D) are a polar molecule. The partial electric charge on each atom in CH_2NH and H_2O are calculated and shown in supporting information Figure S2. Based on charges, we expect they will bind to each other and formed a weakly bound complex i.e., $CH_2NH\cdots H_2O$. The calculated binding energies of $CH_2NH\cdots H_2O$ is 4.4 kcal mol^{-1} lower than the reactants and is also in very good agreement with previous studies[15,16,23]. A hydrogen atom transfer from the H_2O to methylenimine to form an aminomethanol via four-membered transition state TS1 (Fig. 1). The barrier heights for this transformation is 46.4 kcal/mol, which is 8.2 kcal/mol higher than H_2O addition to C=O of $H_2C=C=O$ and 12.3 kcal/mol higher than H_2O addition to C=C bond of $H_2C=C=O$[28]. Once aminomethanol is produced, it can either lose H_2O molecule to regenerate methylenimine or leads to another hydrogen migration via transition state TS3 to form formaldehyde and ammonia. The barrier heights for the formation of formaldehyde and ammonia is also high (30.8 kcal/mol). This value is also in good agreement with Riffet et al. value[15].

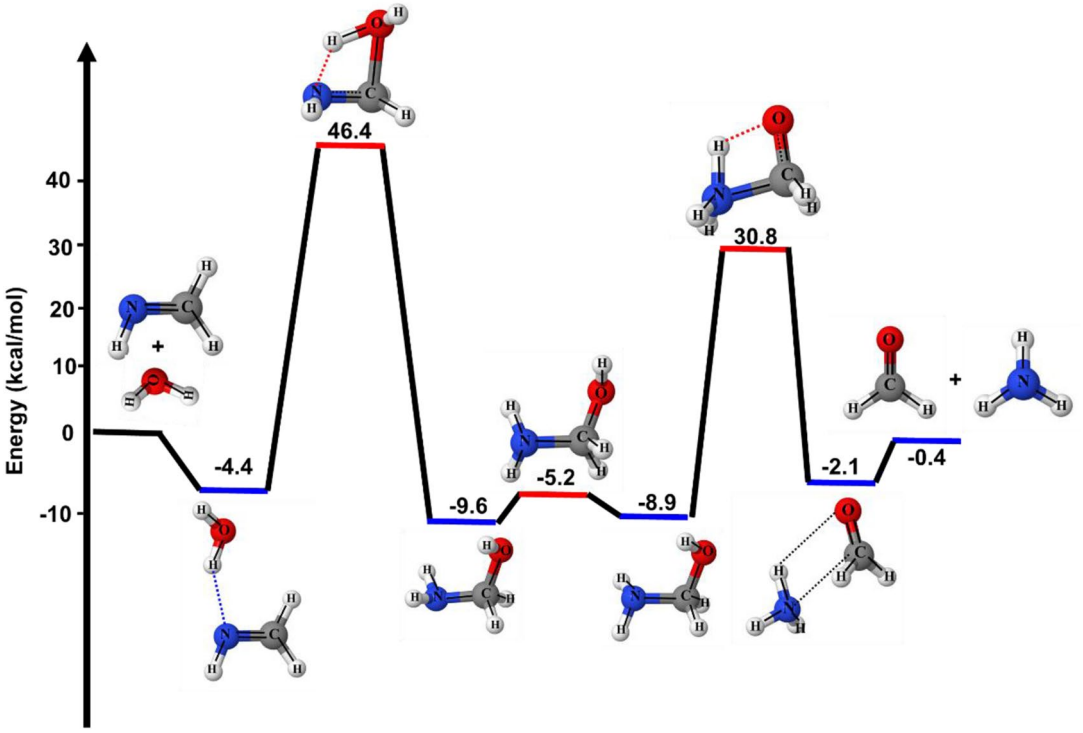

Figure 1. The stationary points on the PES for $CH_2NH + H_2O$ reaction were obtained using CCSD(T)/6–311++G(3df,3pd)//M06-2X/6–311++G(3df,3pd). The relative energies include ZPE corrections are relative to $CH_2NH + H_2O$.

The zero-point corrected PES for $CH_2NH + 2H_2O$ reaction is shown in Fig. 2 and relative energies are tabulated in Table 1. In the presence of two-water molecules, the simultaneous collision of isolated CH_2NH, H_2O and H_2O molecule is very unlikely, therefore, the reaction will occur through the formation of two body complex and then two body complex collides with a third species to form the three-body complex. The calculated binding energies of two body complex i.e., $CH_2NH\cdots H_2O$ (− 4.4 kcal/mol) are in very good agreement with previously reported (− 3.8, − 4.7 kcal/mol)[15,23,24] value . The value for $H_2O\cdots H_2O$ (− 2.9 kcal/mol) are also in very good agreement with Louie et al.[30] (− 3.1 kcal/mol) value. As shown in Fig. 2, beginning with the $H_2O + CH_2NH\cdots H_2O$ or $CH_2NH + H_2O\cdots H_2O$ reactions, a three-body complex $H_2O\cdots CH_2NH\cdots H_2O$ is formed with the additional water molecule acting as both hydrogen bond acceptor and donor, depending on the approach of the hydrogen atoms in the H_2O and CH_2NH molecules. The large binding energies of $H_2O\cdots CH_2NH\cdots H_2O$ (~ 12 kcal/mol) is due to the combined effects of two O···H and one N···H hydrogen bonds. The energies of this complex are also in good agreement with Riffet et al. value[15]. It is obvious that water molecule can not only act as reactants but also play an important catalytic role, which makes reaction more thermodynamically feasible (see Fig. 2).

As shown in Fig. 2, the reaction proceeds through a transition state ($TS1\cdots H_2O$), with a barrier of ~ 21 kcal/mol (with respect $CH_2NH + 2H_2O$) to form an aminomethanol$\cdots H_2O$. In this process, the six-membered transition state ($TS1\cdots H_2O$), which has considerably less strain than that of four-membered TS1 of $CH_2NH + H_2O$ reaction. The two-water reaction significantly reduced the activation barrier by 25.0 kcal/mol. This result is also consistent with the previous studies on similar reaction system[28,30]. Similar to the one-water reaction, aminomethanol can react catalytically with a single water molecule to either regenerate methylenimine or to form formaldehyde. The barrier heights for the formation of formaldehyde and ammonia is lower (7.6 kcal/mol), and thus should be the dominant channel. As a result, when the aminomethanol is formed, it will rapidly decompose to formaldehyde and ammonia in the presence of water.

Based on the energetics summarized in Table 1, the first barrier heights of a single water reaction is very high (46 kcal/mol). In the case of two water reactions, one water molecule is acting as a catalyst and still does not reduce the barrier heights sufficiently low to allow the hydrolysis of methylenimine to occur readily under typical atmospheric conditions. It has been also reported in the literature that the addition of more water molecules further decreases the barrier heights, but such reactions are not likely to occur in the gas phase[15,28,29]. As discussed in ketene + H_2O reaction[28], the gas-phase hydration of ketene by an excess of two water molecules is unlikely to occur at ambient temperatures because the concentration of $(H_2O)_{n>2}$ clusters in the gas-phase is negligibly small under these conditions. Therefore, the reaction of methylenimine with $(H_2O)_{n>2}$ is beyond the scope of the present work.

Chemical kinetics results. *Rate constants.* The $CH_2NH\cdots H_2O$ complex that plays important roles in the $CH_2NH + H_2O$ reaction system are formed via entrance channels that have no intrinsic energy barriers i.e., barrierless. Figure 3 shows the zero-point corrected potential energy for the entrance channel forming $CH_2NH\cdots H_2O$.

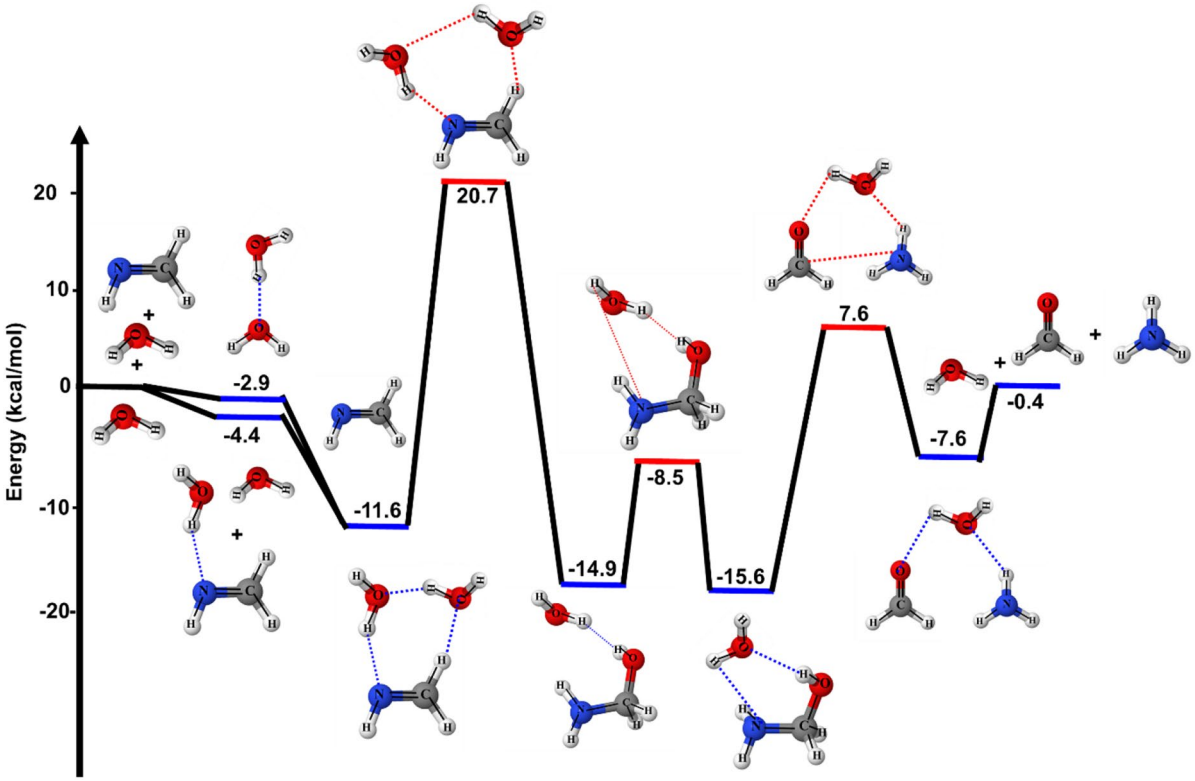

Figure 2. The stationary points on the PES for $CH_2NH + H_2O + H_2O$ reaction were obtained using CCSD(T)/6–311++G(3df,3pd)//M06-2X/6–311++G(3df,3pd). The relative energies include ZPE corrections are relative to $CH_2NH + 2H_2O$.

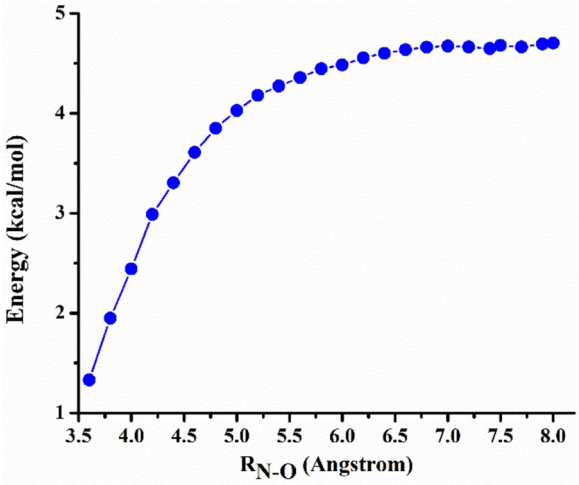

Figure 3. Zero-point corrected potential energy profile for the dissociation of the $CH_2NH\cdots H_2O$ as functions of $R_{N\text{-}O}$ distances.

To locate the transition state for the dissociation of $CH_2NH\cdots H_2O$, the potential energies (including zero-point energies) were computed in a series of constrained optimizations "trial TS" have one fixed frequency and remaining orthogonal frequency are properly projected as a function of the $R_{N\text{-}O}$ bond distance (from 3 to 8 Å). The optimized geometries at some points along the reaction pathways are shown in Fig. 4. All the transition states shown in Fig. 4 have a single imaginary frequency and the normal modes of vibration of these transition states were confirmed to be reliable with the reaction of interest through visualization with GaussView.

At $R_{N-O} = 8$ Å, the interactions between CH_2NH and H_2O are very weak. As the two species approach one another, the potential energy decreases monotonically until it reaches the bottom of the potential well (Fig. 3). The PES decreases to ~ 1 kcal/mol at $R_{N-O} = 4$ Å and decreased further as CH_2NH and H_2O come close to each other. The CVTST "trial" rate constants computed in the temperature range of 200–400 K along the reaction path

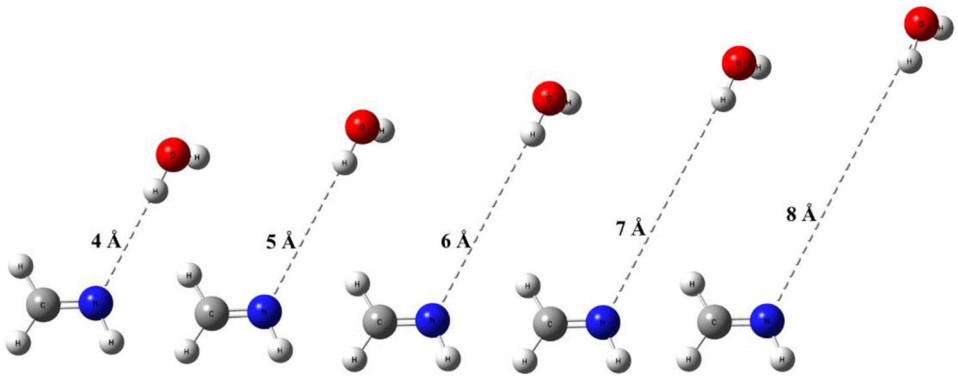

Figure 4. "Trial" TSs of $CH_2NH + H_2O$ reaction at several R_{N-O} distances along the reaction pathway forming $CH_2NH\cdots H_2O$.

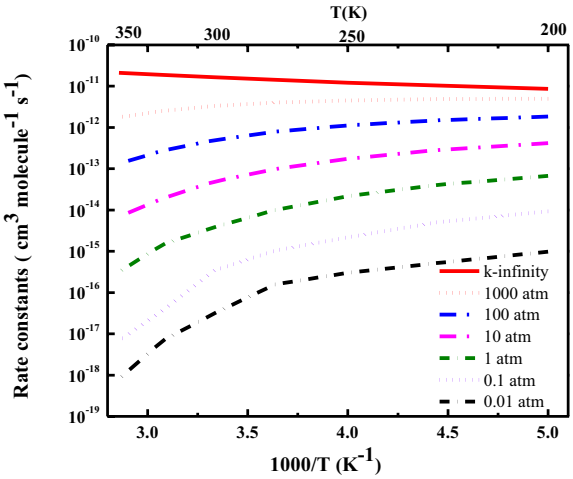

Figure 5. Temperature-and pressure-dependent rate constants for $CH_2NH + H_2O \rightarrow CH_2NH\cdots H_2O$.

are shown in Supporting Information Figure S4. At each temperature, the plot shows a single minimum between 5.8 to 6.6 Å. The rate constants for dissociation and association reaction were computed using both canonical and microcanonical approaches and values are tabulated in Supporting Information, Table S7. Our calculation shows that both canonical and microcanonical rate constants for $CH_2NH + H_2O \rightarrow CH_2NH\cdots H_2O$ reaction is very similar. It is also interesting to know that rate of formation of $CH_2NH\cdots H_2O$ increases as temperature increases.

The sum of states obtained from μVTST process was used to run the master equation (ME) code for pressure-dependent (*i.e.,* falloff curve) rate constants. Figure 5 shows that microcanonical chemical activation k (E,J) for $CH_2NH + H_2O$ reaction as a function of temperature (200–350 K) and pressure (0.01–1,000 atm). The rate constants are pressure-dependent and show negative temperature-dependence. At lower pressure, rate constants decrease with an increase in temperature and are almost independent of temperature at high-pressure limit. ME simulations show that the formation of $CH_2NH\cdots H_2O$ is dominant under all the conditions investigated and all other channels i.e., CH_2NH_2OH, $CH_2O\cdots NH_3$ and $CH_2O + NH_3$ are almost negligible. This result is due to the fact that the barrier heights for the formation of CH_2NH_2OH, $CH_2O\cdots NH_3$ and $CH_2O + NH_3$ are significantly higher. Our results also suggest that rate constants at high-pressure limit have positive temperature-dependence. This result is similar to the $OH + CO$ and $H + O_2$ reaction systems (see examples posted on the MultiWell web site) and the result obtained previously for the $CH_2O + NH_3$ reaction system[20]. We believe that the current microVTST results are accurate to within about a factor of 2.

In some cases, where the rate constant is pressure-independent or depends only weakly on pressure, one does not need to solve ME numerically, and an analytical solution can be obtained. As suggested in earlier studies for a similar reaction system i.e., $H_2O + H_2C{=}C{=}O$, the formation of products is almost pressure-independent[28,29], therefore the rate constants for the reactions of methylenimine with one and two water molecules were calculated based on the high-pressure limit condition as discussed in the method section. The rate constants for the reactions of methylenimine with one water and two water molecules were calculated as a function of temperature are tabulated in Table 2 and shown in Fig. 6.

As discussed in "Reaction pathways and thermodynamics analysis", reactions of methylenimine with two-water molecules proceeds through a seven-membered complex, followed by H_2O addition leading to products.

Temp (K)	$CH_2NH + H_2O \rightarrow CH_2O + NH_3$	$CH_2NH + H_2O\cdots H_2O \rightarrow CH_2O + NH_3 + H_2O$	$CH_2NH\cdots H_2O + H_2O \rightarrow CH_2O + NH_3 + H_2O$	Total effective rate constants (k_p)
500	1.6×10^{-33}	1.1×10^{-26}	3.8×10^{-26}	4.0×10^{-32}
600	1.7×10^{-30}	3.1×10^{-25}	1.3×10^{-24}	8.4×10^{-31}
700	3.6×10^{-28}	3.9×10^{-24}	1.9×10^{-23}	9.1×10^{-30}
800	2.1×10^{-26}	2.8×10^{-23}	1.6×10^{-22}	6.1×10^{-29}
900	5.3×10^{-25}	1.3×10^{-22}	8.4×10^{-22}	3.0×10^{-28}
1,000	7.5×10^{-24}	4.9×10^{-22}	3.3×10^{-21}	1.1×10^{-27}
1,100	6.7×10^{-23}	1.5×10^{-21}	1.1×10^{-20}	3.6×10^{-27}
1,200	4.3×10^{-22}	3.9×10^{-21}	2.9×10^{-20}	9.9×10^{-27}
1,300	2.1×10^{-21}	8.9×10^{-21}	7.0×10^{-20}	2.4×10^{-26}
1,400	8.5×10^{-21}	1.9×10^{-20}	1.5×10^{-19}	5.5×10^{-26}
1,500	2.9×10^{-20}	3.6×10^{-20}	3.0×10^{-19}	1.1×10^{-25}
1,600	8.5×10^{-20}	6.4×10^{-20}	5.6×10^{-19}	2.2×10^{-25}
1,700	2.2×10^{-19}	1.1×10^{-19}	9.8×10^{-19}	4.2×10^{-25}
1,800	5.3×10^{-19}	1.8×10^{-19}	1.6×10^{-18}	7.4×10^{-25}
1900	1.2×10^{-18}	2.8×10^{-19}	2.6×10^{-18}	1.3×10^{-24}
2000	2.4×10^{-18}	4.2×10^{-19}	4.0×10^{-18}	2.1×10^{-24}
$k = AT^n Exp(-Ea/RT)$	$A = 3.6\times10^{-29}$, n = 4.6, Ea/R = 1.9×10^4	$A = 9.5\times10^{-31}$, n = 4.0, Ea/R = 7.9×10^3	$A = 1.2\times10^{-59}$, n = 4.1, Ea/R = 8.6×10^3	$A = 4.3\times10^{-46}$, n = 6.9, Ea/R = 5.41×10^3

Table 2. Rate constants (cm^3 $molecule^{-1}$ s^{-1}) for $CH_2NH + H_2O \rightarrow CH_2O + NH_3$ and $CH_2NH\cdots H_2O + H_2O \rightarrow CH_2O + NH_3 + H_2O$ (Pathway A) and $CH_2NH + H_2O\cdots H_2O \rightarrow CH_2O + NH_3 + H_2O$ (Pathway B).

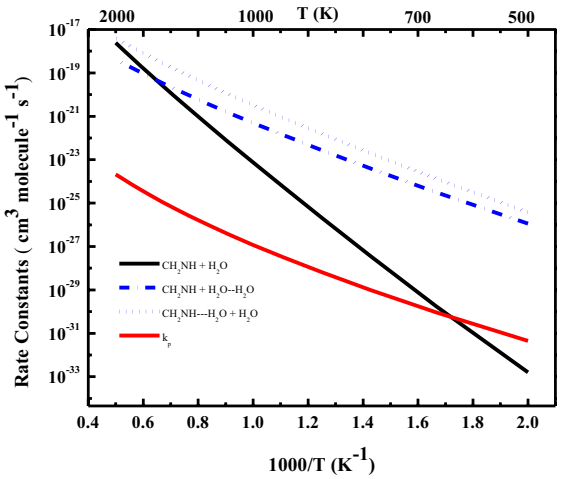

Figure 6. Rate constants for the reaction of methylenimine with one-water and two-water molecules. Dash lines correspond to reaction without water-concentration. It should be noted that these are infinite pressure limit rate constants, which are assumed to be valid from the range $T \geq 300$ K, and $p \geq 1$ atm.

The possibility of the termolecular reaction (i.e., one methylenimine and two free water molecules come together to collide at the same time) is very small under realistic conditions[23,24,28], therefore, either a N–H hydrogen-bonded $CH_2NH\cdots H_2O$ complex or a O–H hydrogen-bonded $H_2O\cdots H_2O$ complex is expected to form first, followed by an attack of the third molecule (H_2O) to this nascent complex and leading to the following important bimolecular reactions:

Pathway A

Step 0A

$$CH_2NH + H_2O \xrightarrow{k_{0A}} CH_2NH\cdots H_2O$$

$$CH_2NH\cdots H_2O \xrightarrow{k_{-0A}} CH_2NH + H_2O$$

Step 1_A

$$CH_2NH\cdots H_2O + H_2O \xrightarrow{k_{1A}} H_2O\cdots CH_2NH\cdots H_2O$$

$$H_2O\cdots CH_2NH\cdots H_2O \xrightarrow{k_{-1A}} CH_2NH\cdots H_2O + H_2O$$

Step 2_A

$$H_2O \cdots CH_2NH \cdots H_2O \xrightarrow{k_{2A}} \text{Products}$$

Pathway B

Step 0_B

$$H_2O + H_2O \xrightarrow{k_{0B}} H_2O \cdots H_2O$$

$$H_2O \cdots H_2O \xrightarrow{k_{-0B}} H_2O + H_2O$$

Step 1_B

$$H_2O \cdots H_2O + CH_2NH \xrightarrow{k_{1B}} H_2O \cdots CH_2NH \cdots H_2O$$

$$H_2O \cdots CH_2NH \cdots H_2O \xrightarrow{k_{-1B}} H_2O \cdots H_2O + CH_2NH$$

Step 2_B

$$H_2O \cdots CH_2NH \cdots H_2O \xrightarrow{k_{2B}} \text{Products}$$

As discussed in earlier works[23,24], locating the TS of backward reaction (i.e., PRC → $CH_2NH + H_2O \cdots H_2O$ or PRC → $CH_2NH \cdots H_2O + H_2O$) is more difficult due presence of two or more hydrogen bonds in PRCs, therefore, the equilibrium approach was used to account the presence of forward and backward reactions. This model is reasonably correct when the pre-reactive complex can be stabilized by collisions with other atmospheric species. This approach has been widely used in the literature for the water-assisted reaction and predicted rate constants that are in reasonably good agreement with literature value[23,24].

As suggested by the reviewer, we have also carried out temperature-and pressure-dependent rate constant calculations for two-water reaction using ME method and results are shown in the supporting information Figure S6. Because of the complexity in locating the TS of loose bonds due to the presence many hydrogens bonded complex in the PRC, we have used Inverse Laplace Transform (ILT) method to account for the barrierless reaction. The ILT parameters used in our calculation are based on our previous work i.e., $CH_2NH + HO_2 \rightarrow CH_2NH \cdots HO_2$. Because the first barrier heights is too high (i.e., 32 kcal/mol w.r.t. PRC, see Fig. 2) our ME calculation suggests that the formation of other species (Intermediates and products) are negligibly small in all the temperature and pressure range studied. Based on ME simulation, we have observed that the infinite pressure condition k (T,p), with T ≥ 300 and p ≥ 1 atm for the two-water reaction.

The bimolecular rate constants of pathway A and pathway B were calculated using $k_A = K_{eq(A)} \times k_A^{CVT}$ and $k_B = K_{eq(B)} \times k_B^{CVT}$, respectively. The rate constants for these pathways are tabulated in Table 2 and shown in Fig. 6. As shown in the Fig. 6 and tabulated in Table 2, the kinetics of the two-water reaction is more favorable than one-water reaction. This result is due to the fact that the barrier heights of two-water reaction are significantly lower than one-water reaction. As expected, pathway A is more kinetically favorable than pathway B. This result is due to the formation of strong N–H hydrogen-bonded complex ($CH_2NH \cdots H_2O$) than weak O–H hydrogen-bonded complex $H_2O \cdots H_2O$, which is also consistent with our previous studies[23,24]. It can be seen from Fig. 6, the rate constants for $CH_2NH \cdots H_2O + H_2O$ and $CH_2NH + H_2O \cdots H_2O$ at < 1000 K are larger than the $CH_2NH + H_2O$ reaction and the difference becomes smaller as the temperature increases and is almost similar at the higher temperature (~ 2000 K). It is also clear from this analysis that all reactions involving additional catalytic water are entirely negligible at high temperatures.

The calculated rate constants predict the positive temperature-dependence i.e., rate constants increase with the increase of temperature (see Fig. 6). The tunneling correction for single water and two-water reactions are tabulated in Supporting Information, Table S8. It can be seen from Table S8 (a), the tunneling correction decreases with temperature and at temperature > 1500 K, tunneling correction is almost negligible i.e., Γ = 1. In other words, at the combustion condition where the formation of $CH_2O + NH_3$ occurred, tunneling is almost negligible. This result is consistent with previous work on similar reaction system[28]. The tunneling correction of two water reaction is greater than one water reaction at lower temperature and almost negligible at temperature > 1300 K (see Table S8 (b). It should be noted that the $k(T)$ given in Table 2 has a non-Arrhenius behaviour because of quantum mechanical tunneling effects.

The effective bimolecular rate constants were calculated using with water concentration, which is based on previous works[23,55,56], therefore the correct expression to calculate the effective rate constants of pathway A and pathway B is given in Eqs. (8) and (9), respectively:

$$k_A^{eff} = K_{eq(CH_2NH--H_2O)} \times k_A \times [H_2O] \tag{8}$$

$$k_B^{eff} = K_{eq(H_2O--H_2O)} \times k_B \times [H_2O] \tag{9}$$

$K_{eq(CH_2NH--H_2O)}$ and $K_{eq(H_2O--H_2O)}$ are equilibrium constants for $CH_2NH + H_2O \rightarrow CH_2NH \cdots H_2O$ and $H_2O + H_2O \rightarrow H_2O \cdots H_2O$, reactions, respectively (see Supporting Information, Table S4). The k_A and k_B are the bimolecular rate constants of pathway A and pathway B (see Table 2). The $[H_2O]$ concentration ~ 7.5×10^{16} molecule/cm^3 was used in our calculation is based on the previous study[28]. As shown in Fig. 2, the kinetic scheme

$CH_2NH + H_2O + H_2O \rightarrow CH_2NH\cdots H_2O\cdots H_2O \rightarrow$ Products, the rate-determining step is at step 2, which is the same in both pathways. Therefore, the correct equation to calculate the total effective rate constants (k_P) is expressed by Eq. 10

$$k_P = k_A^{eff} = k_B^{eff} \tag{10}$$

As shown in Fig. 6 and given in Table 2, that effective rate constant at 500 K is five times larger than the one-water reaction. This result suggests that catalytic reaction takes place at a temperature ≤ 500 K. In general, the effective rate constants of the two-water reaction are smaller than the single-water reaction system in the temperature range of 600–2000 K. As a result, $H_2O + CH_2NH$ reaction catalyzed by another H_2O molecule play a minor role for the sink of CH_2NH in gas phase combustion reaction. Unfortunately, experimental data are not available to validate our predicted rate constants. But we have examined the consistency of present work with earlier theoretical works on similar reaction system[28]. For that purpose, we have calculated the rate constants for termolecular $CH_2NH + H_2O + H_2O \rightarrow CH_2O + NH_3 + H_2O$ reaction and compared the result with $CH_2CO + H_2O + H_2O \rightarrow CH_3COOH + H_2O$ reaction (see Figure S5)[28]. Our calculated rate constants for $CH_2NH + H_2O + H_2O$ reaction are in good with the value of $CH_2CO + H_2O + H_2O$ reaction in the temperature range of 500–2000 K (see Figure S5).

Atmospheric and combustion implications. As reported in previous studies that the methylenimine are likely to hydrolyze easily under atmospheric conditions and hydrolysis of methylenimine will produce $NH_3 + CH_2O$[1,15,27]. It is our interest to know whether or not formaldehyde and ammonia can be produced from the reaction of methylenimine with a single-water and two-water molecules. For this reason, we calculated the pseudo-first-order rate constants for the decay of methylenimine at 1500 K. The water concentration of $[H_2O] \sim 7.5 \times 10^{16}$ molecule cm^{-3} at 50% of relative humidity was used in calculation[28]. The calculated lifetime of methylenimine is ~8 min within a factor of 2 errors. The calculated lifetime of methylenimine (~8 min.) is also in good agreement with the lifetime of ketene i.e., ~5 min. Our calculations suggest that methylenimine can convert to formaldehyde and ammonia only under the combustion condition.

It is important to mention that the reaction of $H_2O + CH_2NH$ is still slower than other important reactions for example radical-molecules reaction i.e., $CH_2NH + OH$, $CH_2NH + HO_2$ and $CH_2NH + OH$ (+ H_2O). Based on our previous works, the $CH_2NH + OH$ reaction is faster than the $H_2O + CH_2NH$ in both atmospheric and combustion conditions[21–23]. The estimated timescales of 8 min are too large to be competitive with the fast-radical reactions i.e., $CH_2NH + OH$ (+ H_2O) ~ 1 ns. Therefore, we believe the kinetic of $H_2O + CH_2NH$ is even slow in the combustion process compared to radical molecule reactions. Experimental studies are required to validate the formation of CH_2O and NH_3 from $CH_2NH + H_2O$ reaction.

Now it is important to address the question of whether two-water molecules reaction can produce the formaldehyde and ammonia under atmospheric condition. To understand that, we calculated the pseudo-first-order reaction rate decay of methylenimine at 300 K and at $[H_2O] = 7.1 \times 10^{17}$ molecule/cc at 100% relative humidity. The calculated decay rate is $\sim 4.2 \times 10^{11}$ s^{-1} suggest that two-water molecule reaction to form formaldehyde and ammonia is even slower. Therefore, the reaction of two-water molecules on methylenimine cannot produce formaldehyde and ammonia under atmospheric conditions[1].

To investigate the possibility of the secondary atmospheric reaction with $CH_2NH\cdots H_2O$, the atmospheric lifetime of $CH_2NH\cdots H_2O$ at 225 K and 0.1 atm (i.e., at an altitude of ~ 10–11 km) were calculated and found to be ~ 10 ms. This is a too short lifetime for $CH_2NH\cdots H_2O$ to undergoes significant bimolecular reactions with other atmospheric species. Thus, although this is an interesting complex, our pressure-dependent rate constants calculation suggests that its formation under the atmospheric condition is unimportant.

Our observation shows that room-temperature formation of formaldehyde and ammonia cannot have come from either of the mechanism of one-water and two-water reaction under atmospheric conditions. Hence, either another mechanism exists or surface reactions similar to that was observed previously are responsible for the formation of formaldehyde and ammonia[28] The present finding is also consistent with previous studies on the similar type of reactions[28,29].

Conclusions

The potential energy surfaces and rate constants for the reaction of methylenimine with one-water and two-water molecules in the gas phase reaction have been calculated using CCSD(T)/M06-2X with 6–311++G(3df,3pd) basis set. For barrierless reactions, rate constants were calculated using canonical and microcanonical variational transition state theory coupled with RRKM/ME simulations and for non-barrierless reactions CVT/SCT approach was used to compute the rate constants. The relative energies of stationary points on the PES are in good agreement with previous values. The barrier heights of one-water reaction are very high. When an additional water molecule is added to the reaction, barrier heights significantly reduced by 25 kcal/mol. Therefore, we can say that an additional water molecule plays a role of a catalysis.

The rate constants for the formation of $CH_2NH\cdots H_2O$ is both temperature-and pressure-dependent. At the high-pressure limit, the formation of $CH_2NH\cdots H_2O$ shows weak positive temperature-dependence. Because the lifetime $CH_2NH\cdots H_2O$ is too short, it is expected to play a negligible role in the atmosphere.

The one-water reaction is to form formaldehyde and ammonia (within a few minutes) is dominant at high temperatures, whereas the two-water reaction becomes the major channel at a lower temperature if step 0 is not included in the calculation. Ignoring step 0 is equivalent to assuming that all the methylenimine is complexed with water, which is not true. Therefore, the correct reaction pathways should have $[H_2O]$ in the rate constants calculations. In that case, our calculations demonstrate that two-water reaction has the potential to accelerate a

gas phase reaction ≤ 500 K, but the rate of formation of formaldehyde and ammonia is predicted to be negligibly slow. This result is also consistent with previous studies on the similar reaction system, i.e., $H_2O + H_2C=C=O$. Experimental studies are required to understand the formation of CH_2O and NH_3 from $CH_2NH + H_2O$, and other formation schemes must be explored. Once the laboratory characterization is complete, CH_2O and NH_3 will be an ideal target for observational search. Although this is an interesting reaction system, our results demonstrate that $CH_2NH + H_2O$ is not important under atmospheric and combustion conditions compared to an important radical molecule reaction. Such results are encouraging, and chemical kinetic mechanism can be useful for the future implementation of hydrolysis of other imine compounds.

Data availability

All data generated through this study are given in the Supporting Information file. Supporting Information: Tables of optimized geometries, rotational-vibrational parameters, electronic energies, zero-point energies of all the species involved in the $CH_2NH + H_2O$ and $CH_2NH + 2H_2O$ reactions. Tables of T1 diagnostic for all the species, equilibrium constants, tunneling corrections and rate constants. Figures of optimized structures and comparison of rate constants with other study. Temperature -and pressure-dependent rate constant for one water and two-water reaction. Details discussion on the methodology. Input files for THERMO and KTOOLS are given for replicating the present work.

Received: 11 December 2019; Accepted: 31 May 2020
Published online: 03 July 2020

References

1. Nielsen, C. J., Herrmann, H. & Weller, C. Atmospheric chemistry and environmental impact of the use of amines in carbon capture and storage (CCS). *Chem. Soc. Rev.* **41**, 6684–6704 (2012).
2. Hao, W. M., Scharffe, D. H., Lobert, J. M. & Crutzen, P. J. Emissions of nitrous oxide from the burning of biomass in an experimental system. *Geophys. Res. Lett.* **18**, 999–1002 (1991).
3. Schade, G. W. & Crutzen, P. J. Emission of aliphatic amines from animal husbandry and their reactions: potential source of N_2O and HCN. *J. Atmos. Chem.* **22**, 319–346 (1995).
4. Quinto-Hernandez, A. *et al.* On the interaction of methyl azide (CH_3N_3) ices with ionizing radiation: formation of methanimine (CH_2NH), hydrogen cyanide (HCN), and hydrogen isocyanide (HNC). *J. Phys. Chem. A* **115**, 250–264 (2011).
5. Dana, A. G., Elishav, O., Bardow, A., Shter, G. E. & Graden, G. S. Nitrogen-based fuels: a power-to-fuel-to-power analysis. *Angew. Chem. Int. Ed.* **55**, 8798–8805 (2016).
6. Zhan, H., Zhuang, X., Song, Y., Yin, X. & Wu, C. Insights into the evolution of fuel-N to NO_x precursors during pyrolysis of N-rich nonlignocellulosic biomass. *Appl. Energ.* **219**, 20–33 (2018).
7. Yu, G. & Luo, G. Modeling of gaseous methylamines in the global atmosphere: impacts of oxidation and aerosol uptake. *Atmos. Chem. Phys.* **14**, 12455–12464 (2014).
8. Ge, X., Wexler, A. S. & Clegg, S. L. A. Atmospheric amines—part I. A review. *Atmos. Environ.* **45**, 524–546 (2011).
9. Onel, L., Blitz, M., Dryden, M. B., Thonger, L. & Seakins, P. Branching ratios in reactions of OH radicals with methylamine, dimethylamine, and ethylamine. *Environ. Sci. Technol.* **48**, 9935–9942 (2014).
10. Rissanen, M. P. *et al.* $CH_2NH_2 + O_2$ and $CH_3CHNH_2 + O_2$ reaction kinetics: photoionization mass spectrometry experiments and master equation calculations. *J. Phys. Chem. A* **118**, 2176–2186 (2014).
11. Bernstein, M. P., Bauschlicher, C. W. Jr. & Sandford, S. A. The infrared spectrum of matrix isolated aminoacetonitrile, a precursor to the amino acid glycine. *Adv. Space Res.* **33**, 40–43 (2004).
12. Koch, D. M., Toubin, C., Peslherbe, G. H. & Hynes, J. T. A. Theoretical study of the formation of the aminoacetonitrile precursor of glycine on icy grain mantles in the interstellar medium. *J. Phys. Chem. C.* **112**, 2972–2980 (2008).
13. Dyke, J. M. *et al.* Moutinho, study of the thermal decomposition of 2-azidoacetic acid by photoelectron and matrix isolation infrared spectroscopy. *J. Am. Chem. Soc.* **119**, 6883–6887 (1997).
14. Pearson, R. Jr. & Lovas, F. J. Microwave spectrum and molecular structure of methylenimine (CH_2NH). *J. Chem. Phys.* **66**, 4149–4156 (1997).
15. Riffet, V., Frison, G. & Bouchoux, G. Quantum-chemical modeling of the first steps of the strecker synthesis: from the gas-phase to water solvation. *J. Phys. Chem. A* **122**, 1643–1657 (2018).
16. Feldmann, M. T. *et al.* Aminomethanol water elimination: theoretical examination. *J. Chem. Phys.* **123**, 034304 (2005).
17. Walch, S. P., Bauschlicher, C. W., Ricca, A. & Bakes, E. L. O. On the reaction $CH_2O + NH_3 = CH_2NH + H_2O$. *Chem. Phys. Lett.* **333**, 6–11 (2001).
18. Ćmikiewicz, A., Gordon, A. J. & Berski, S. Characterisation of the reaction mechanism between ammonia and formaldehyde from the topological analysis of ELF and catastrophe theory perspective. *Struct. Chem.* **29**, 243–255 (2018).
19. Woon, D. E. Ab Initio quantum chemical studies of reactions in astrophysical ices 2. Reactions in $H_2CO/HCN/HNC/H_2O$ Ices. *Icarus* **149**, 277–284 (2001).
20. Ali, M. A. Theoretical study on gas phase reaction of CH_2O+NH_3: formation of $CH_2O\cdots NH_3$, NH_2CH_2OH, or $CH_2NH + H_2O$. *Phys. Chem. Chem. Phys.* **21**, 19242–19251 (2019).
21. Ali, M. A. & Barker, J. R. Comparison of three isoelectronic multiple-well reaction systems: OH + CH_2O, OH + CH_2CH_2, and OH + CH_2NH. *J. Phys. Chem. A* **119**, 7578–7592 (2015).
22. Ali, M. A., Sonk, J. A. & Barker, J. R. Predicted chemical activation rate constants for HO_2 + CH_2NH: the dominant role of a hydrogen-bonded pre-reactive complex. *J. Phys. Chem. A* **120**, 7060–7070 (2016).
23. Ali, M. A., Balaganesh, M. & Lin, K. C. Catalytic effect of a single water molecule on the OH + CH_2NH reaction. *Phys. Chem. Chem. Phys.* **20**, 4297–4307 (2018).
24. Ali, M. A., Balaganesh, M. & Jang, S. Can a single water molecule catalyze the OH+CH_2CH_2 and OH+CH_2O reactions?. *Atmos. Environ.* **207**, 82–92 (2019).
25. Bunkan, A. J. C., Tang, Y., Sellevag, S. R. & Nielsen, C. J. Atmospheric gas phase chemistry of CH_2=NH and HNC, a first principle approach. *J. Phys. Chem. A* **118**, 5279–5288 (2014).
26. Vazart, F., Calderini, D., Puzzarini, C., Skouteris, D. & Barone, V. State-of-the-art thermochemical and kinetic computations for astrochemical complex organic molecules: formamide formation in cold interstellar clouds as a case study. *J. Chem. Theory Comput.* **12**, 5385–5397 (2016).
27. Da Silva, G. Atmospheric chemistry of 2-aminoethanol (MEA): reaction of the NH_2·$CHCH_2OH$ radical with O_2. *J. Phys. Chem. A* **116**, 10980–10986 (2012).

28. Nguyen, T. L., Xue, B. C., Ellison, G. B. & Stanton, J. F. Theoretical study of reaction of ketene with water in the gas phase: formation of acetic acid?. *J. Phys. Chem. A.* **43**, 10997–11005 (2013).
29. Kahan, T. F., Ormond, T. K., Ellison, G. B. & Vaida, V. Acetic acid formation via the hydration of gas-phase ketene under ambient conditions. *Chem. Phys. Lett.* **565**, 1–4 (2013).
30. Louie, M. K. *et al.* Hydrolysis of ketene catalyzed by formic acid: modification of reaction mechanism, energetics, and kinetics with organic acid catalysis. *J. Phys. Chem. A* **119**, 4347–4357 (2015).
31. Zhao, Y. & Truhlar, D. G. The M06 suite of density functionals for main group thermochemistry, thermochemical kinetics, noncovalent interactions, excited states, and transition elements: two new functionals and systematic testing of four M06-class functionals and 12 other functionals. *Theor. Chem. Acc.* **120**, 215–241 (2008).
32. Frisch, M. J., Pople, J. A. & Binkley, J. S. Self-consistent molecular orbital methods supplementary functions for gaussian basis sets. *J. Chem. Phys.* **80**, 3265–3269 (1984).
33. Parandaman, A., Tangtartharakul, C. B., Kumar, M., Francisco, J. S. & Sinha, A. A computational study investigating the energetics and kinetics of the HNCO + $(CH_3)_2NH$ reaction catalyzed by a single water molecule. *J. Phys. Chem. A* **121**, 8465–8473 (2017).
34. Abdel-Rahman, M. A. *et al.* Computational studies on the thermodynamic and kinetic parameters of oxidation of 2-methoxyethanol biofuel via H-atom abstraction by methyl radical. *Sci. Rep.* **9**, 15361 (2019).
35. Ji, Y. *et al.* OH-initiated oxidation of acetylacetone: implications for ozone and secondary organic aerosol formation. *Environ. Sci. Technol.* **52**, 11169–11177 (2018).
36. Raghavachari, K., Trucks, G. W., Pople, J. A. & Head-Gordon, M. A fifth-order perturbation comparison of electron correlation theories. *Chem. Phys. Lett.* **157**, 479–483 (1989).
37. Woon, D. E. & Dunning, T. H. Gaussian basis sets for use in correlated molecular calculations. III. The atoms aluminum through argon. *J. Chem. Phys.* **98**, 1358 (1993).
38. Kumar, M. & Francisco, J. S. H–X (X = H, CH_3, CH_2F, CHF_2, CF_3, and SiH_3) bond activation by Criegee intermediates: a theoretical perspective. *J. Phys. Chem. A* **121**, 9421–9428 (2017).
39. Sheng, F. *et al.* Theoretical study of the oxidation reactions of sulfurous acid/sulfite with ozone to produce sulfuric acid/sulfate with atmospheric implications. *RSC Adv.* **8**, 7988–7996 (2008).
40. Rienstra-Kiracofe, J. C., Allen, W. D. & Schaefer, H. F. I. The $C_2H_5 + O_2$ reaction mechanism: high-level ab initio characterizations. *J. Phys. Chem. A* **104**, 9823–9840 (2000).
41. Frisch, M. J. *et al. Gaussian 09* (Gaussian Inc, Wallingford CT, 2009).
42. Zheng, J. *et al. POLYRATE, version 2008* (University of Minnesota, Minneapolis, 2009).
43. Chuang, Y.-Y., Corchado, J. C. & Truhlar, D. G. Mapped interpolation scheme for single-point energy corrections in reaction rate calculations and a critical evaluation of dual-level reaction path dynamics methods. *J. Phys. Chem. A* **103**, 1140–1149 (1999).
44. Skodje, R. T., Truhlar, D. G. & Garrett, B. C. A general small-curvature approximation for transition state theory transmission coefficients. *J. Phys. Chem. A* **85**, 3019–3023 (1982).
45. Zheng, J. Z. *et al. GAUSSRATE, version 2009-A* (University of Minnesota, Minneapolis, 2010).
46. Barker, J. R. Multiple-well, multiple-path unimolecular reaction systems. I. MultiWell computer program suite. *Int. J. Chem. Kinet.* **33**, 232–245 (2001).
47. Barker, J. R. Energy transfer in master equation simulations: a new approach. *Int. J. Chem. Kinet.* **41**, 748–763 (2009).
48. Barker, J. R. *et al. MultiWell-2016 Software* (University of Michigan, Ann Arbor, 2016).
49. Stein, S. E. & Rabinovitch, B. S. Accurate evaluation of internal energy level sums and densities including anharmonic oscillators and hindered rotors. *J. Chem. Phys.* **58**, 2438–2445 (1973).
50. Beyer, T. & Swinehart, D. F. Number of multiply-restricted partitions. *Commun. Assoc. Comput. Mach.* **16**, 379–379 (1973).
51. Goldsmith, C. F., Green, W. H. & Klippenstein, S. J. Role of O2 + QOOH in low-temperature ignition of propane. 1. Temperature and pressure dependent rate coefficients. *J. Phys. Chem. A* **116**, 3325–3346 (2012).
52. Ruscic, B. *et al.* Introduction to active thermochemical tables: several "key" enthalpies of formation revisited. *J. Phys. Chem.* **108**, 9979–9997 (2004).
53. Ruscic, B. *et al.* Active thermochemical tables: thermochemistry for the 21st century. *J. Phys. Conf. Ser.* **16**, 561–570 (2005).
54. Ruscic, B. & Bross, D. H. Active thermochemical tables (ATcT) enthalpies of formation values based on ver. 1.112d of the thermochemical network (2018).
55. Iuga, C., Alvarez-Idaboy, J. R., Reyes, L. & Vivier-Bunge, A. Can a single water molecule really catalyze the acetaldehyde OH reaction in tropospheric conditions?. *J. Phys. Chem. Lett.* **1**, 3112–3115 (2010).
56. Buszek, R. J., Barker, J. R. & Francisco, J. S. Water effect on the OH + HCl reaction. *J. Phys. Chem. A* **116**, 4712–4719 (2012).

Acknowledgements

Mohamad Akbar Ali (MAA) gratefully acknowledges the Deanship of Scientific Research at King Faisal University, Saudi Arabia for financial support under Nasher Track (Grant no. 186387). MAA thanks Professor D.G. Truhlar for providing the license of Polyrate/GaussRate programs.

Author contributions

M.A.A. prepared figures and tables and draft of the paper. MAA gathered everything, checked the data, discussed it and created it in the final version of the manuscript.

Competing interests

The author declares no competing interests.

Additional information

Supplementary information is available for this paper at https://doi.org/10.1038/s41598-020-67515-3.

Correspondence and requests for materials should be addressed to M.A.A.

Reprints and permissions information is available at www.nature.com/reprints.

Publisher's note Springer Nature remains neutral with regard to jurisdictional claims in published maps and institutional affiliations.

Open Access This article is licensed under a Creative Commons Attribution 4.0 International License, which permits use, sharing, adaptation, distribution and reproduction in any medium or format, as long as you give appropriate credit to the original author(s) and the source, provide a link to the Creative Commons license, and indicate if changes were made. The images or other third party material in this article are included in the article's Creative Commons license, unless indicated otherwise in a credit line to the material. If material is not included in the article's Creative Commons license and your intended use is not permitted by statutory regulation or exceeds the permitted use, you will need to obtain permission directly from the copyright holder. To view a copy of this license, visit http://creativecommons.org/licenses/by/4.0/.

© The Author(s) 2020